Towing-tank tests on a model TLP: Benchmark data for validation of CFD simulations

John R. Chaplin<sup>1</sup> & Bassam A. Younis<sup>2\*</sup>

<sup>1</sup> Faculty of Engineering and the Environment, University of Southampton, Southampton SO17 1BJ,

UK

<sup>2</sup> Department of Civil and Environmental Engineering, University of California, Davis, Davis - CA

95616, USA

**ABSTRACT** 

The purpose of this brief note is to report on the results of an experimental study aimed at

obtaining measurements of the drag on a model Tension Leg Platform (TLP). The motivation

was to provide data suitable for the verification of computational fluid dynamics (CFD)

approaches to the assessment of hydrodynamic loading on full-scale structures. The tests were

carried out in a water flume on a 1:70 scale model TLP consisting of four square pontoons

and four circular cylinders. Results were obtained in steady current at low turbulence

intensity, and for two angles of incidence, namely 0° and 45°. Two different methods were

used to measure the drag with the results corrected to account for wavemaking resistance and

for blockage effects. The Reynolds number in the tests went up to  $Re = 1.06 \times 10^5$ , for

conditions in which the full-scale Reynolds number would be  $Re = 6.2 \times 10^7$ . The results are

briefly discussed and the drag data are tabulated for ease of use.

Keywords: Experimental drag coefficient; verification of CFD software; TLP

\* Corresponding author. E-mail: bayounis@ucdavis.edu.

1

## 1. INTRODUCTION

Recent years have seen a rapid growth in the use of computational fluid dynamics (CFD) to predict the hydrodynamic loads on offshore structures [1-5]. The trend continues, driven by such factors as the seemingly inexorable increase in computer power, the decrease in the cost of finely-resolved computations, and the wide availability of general-purpose CFD software and of associated pre- and post-processing tools. However, the increase in the use of simulations has not been matched by greater availability of experimental data suitable for validating the results. Thus in many computational studies, validation of the computed results is done by reference to experimental data from simple geometries that are often studied in isolation of each other. This makes it difficult to quantify the uncertainty in the prediction of flow around the full-scale structures that are of interest to the offshore engineering community [6]. In particular, the ability of the preferred CFD model to capture the effects of the interactions that occur between the various members of the offshore structures, and the massive separation that occurs downstream of them, remains largely untested and it is these interactions that can significantly alter the magnitude of the hydrodynamic forces that apply. Moreover, since the usual benchmark geometries used in CFD validation are symmetric, the ability to correctly predict the effects of current incidence on the fluid loading cannot be assessed by reference to data from these flows. The purpose of this short paper is to put on record experimental data that may serve as benchmark for validating CFD studies. The data relate to the drag forces on a model Tension Leg Platform (TLP) in steady uniform current at generally low relative levels of turbulence intensity. Results were obtained for two angles of incidence, namely 0° and 45°. In what follows, the experiments are described and the test results are presented and discussed.

## 2. THE EXPERIMENTS

#### 2.1 The model

The experiments were conducted on a 1:70 scale model of the TLP. Figure 1 shows the geometry and defines the coordinates system. The model consisted of four pontoons that are square in section, and four circular columns – their dimensions are given in Table 1. All members were made of 3mm rigid PVC. The columns were terminated at an overall height of 615mm (202mm above the still water level) and joined at the top by a single sheet of 5mm thick plexiglass to provide additional stiffness. The columns and pontoons were sealed to prevent water entry, and the vertical tethers, 2mm diameter stainless steel cables, entered the base of the columns at their centres and passed upwards through internal thin brass tubes. Adjustable clamps attached to the cables where they emerged at the tops of the columns enabled the model to be set horizontally in the water at the appropriate draught with equal tether tensions in each corner. Careful positioning of the clamps also ensured that the tensions in all four tethers were essentially the same.

### 2.2 The towing tank

The tests were carried out in a 55m flume, 1.71m wide that could be operated with water depths up to 1.75m. The flume was equipped with a hydraulically-operated piston-type wave maker, and at the other end with a solid roughened concrete beach with a slope of 1:10. Waves reflected from the beach were of no concern however, since each set of measurements was completed before the reflections would have had time to return to the model. Sufficient time was allowed between tests for the water surface to become almost completely still and for the turbulence that was generated in the previous run to be largely dissipated.

## 2.3 Test layout

The layout for the test is shown in Figure 2. The flume carriage was fitted with a framework made of 50mm steel poles, which extended down to within about 50mm of the tank floor to provide bottom attachment points for the tethers. At the section where the upstream vertical steel poles penetrated the water surface, they were shrouded as shown to minimise the flow disturbance. Tethered in this way, the model was free to undergo large displacements in surge, sway and yaw. To restrict the latter two degrees of freedom, pins were fitted to the

deck of the model to engage loosely between longitudinal guide rails mounted on the carriage. This restricted lateral motion to about  $\pm 2$ mm, but left the model free to respond in surge.

### 2.4 The measurements

Tests to measure the drag of the model in steady currents were carried out by towing the rig through still water at speeds of up to  $0.85 \, \text{m/s}$ , always in the same direction. The model Reynolds number (based on column diameter) was thus  $\text{Re} = 1.06 \times 10^5$  which, based on Froudian scaling wherein  $\text{Re}_{\text{model}} = \text{Re}_{\text{full}} \times \lambda^{3/2}$ , corresponds to conditions in which the full-scale Reynolds number  $\text{Re}_{\text{full}} = 6.2 \times 10^7$ . Between tests the carriage was returned slowly to the starting point, and ample time was then allowed for all detectable motion in the tank to cease.

The tests were completed in two series. In the first, the drag-induced rearwards displacement of the model under tow was measured by a non-intrusive optical system mounted on the carriage above its mid-point. A horizontal tension spring was attached to the model on the upstream side to increase the system's stiffness, and in these conditions the maximum displacement was less than 100mm. The force and displacement calibrations were carried out in still water by loading the model statically in the horizontal direction, and in processing the measurements, account was taken of the resulting slight changes in draught and tether angles. In the second series of tests, the measurements were repeated without the tension spring and displacement transducer, but with a load cell attached to the rear of the model to measure its drag directly. Measurements made in the presence of waves were carried out in this way also. In these two conditions the natural frequencies of the model in surge were 1.12Hz and 14.5Hz respectively. In steady tow cases, the estimated drag on the tethers was subtracted from the measured forces.

## 3. RESULTS

## 3.1 Effect of the free surface on drag

The steady tow tests were carried out at Froude numbers  $F_{\rm r} = V/\sqrt{g} D$  (where V is the towing speed and D the diameter of the columns) of up to about 0.8. In these conditions it is reasonable to expect that the drag would be significantly modified by motion at the free surface around the columns, such as the consequences of a 'bow wave'. To identify this

effect, reference is made to the results of a separate set of measurements described in [7], of the loading on a single vertical surface-piercing cylinder in the near surface region. The difference between the measured drag and that obtained by extending up to the still water surface the loading per unit length observed at large submergences provided a measure of the wavemaking resistance. This can be represented as a point force at the still water level of magnitude  $C_{\rm w} \, {1 \over 2} \, \rho V^2 d^2$  where the coefficient  $C_{\rm w}$  is positive when the effects of the free surface lead to an increase to the overall loading. In figure 3,  $C_{\rm w}$  is plotted against the Froude number, and it can be seen that the wavemaking resistance reaches a maximum at  $F_r \approx 1$ , and that it is negative for Froude numbers in the range 0.4 to 0.64. At  $F_{\rm r}$  = 0.4 the measured pressure distribution on a vertical surface-piercing cylinder was almost unchanged up to the still water level, suggesting that in the range  $F_r < 0.4$  (covering the actual full-scale conditions for the TLP), the wavemaking resistance would be negligible. A polynomial fit to the data shown in figure 3 for  $F_r$  < 1 was therefore used to provide corrections to the measurements of loading on the model TLP in towing tests in still water at  $F_r > 0.4$ , on the assumption that the wavemaking resistance acted only on the front two columns, the rear columns being substantially shielded from the incident flow.

# 3.2 Drag measurements in steady tows in still water at 0° incidence

The measured drag is plotted against the velocity for both series of tests in figure 4, where the data are shown before and after correction for free surface effects discussed above. The result of the corrections is to improve the correlation of the data with straight lines on the graph that correspond to constant drag coefficients ( $C_d = drag / \frac{1}{2} \rho V^2 A$ , A: total projected area). Overall, a good match is found with  $C_d = 1.47$  in the first series of tests, and  $C_d = 1.25$  in the second, in which the natural frequency of the model in surge was much higher. However (as can be seen in figure 4), over a narrow range of velocities from 0.44m/s to 0.49m/s (0.39 <  $F_r$  < 0.44), there was a repeatable and consistent increase in the drag coefficient in the second series of tests, up to a maximum close to that observed in the first, namely 1.47. No other differences were observed in the experiments in this range, except in the output of a wave gauge located on the carriage downstream of the model, and about 0.5m to the side. The measured values of Cd and Re are tabulated in Table 2.

Spectra of water surface elevation records at the wave gauge are shown in figure 5, in which the frequencies f are normalised with respect to the Strouhal frequency  $f_s = SV/D$ , with a Strouhal number S = 0.2. It is seen that over the narrow range of towing velocities in which the increase in  $C_d$  appears in figure 4, there is a marked rise and fall in the content of the wave gauge signal at frequencies close to the Strouhal frequency, suggesting that the increased drag was due to vortex-induced oscillations of the model. The Strouhal frequency was about 0.7Hz, which was far from the model's natural frequency. However, it should be recalled that any lateral motion was constrained to very small amplitudes by the guide rails, and that under these conditions conventional lock-in behaviour may not occur. The maximum wave amplitude at this frequency was about 4mm.

Similar changes were not observed in the measured drag spectra over this range of velocities. Nevertheless it seems reasonable to attribute the difference between drag coefficients obtained from the two series of tests to the large difference in the stiffness of the model system in the two cases. In the first the standard deviation of the displacement in surge during steady tow tests was around 2mm, In the second, based on the standard deviation of the measured force and the stiffness of the load cell, it was less than 1% of this.

# 3.3 Drag measurements in steady tows in still water at 45° incidence

As part of the first series of tests, measurements were made with the model at  $45^{\circ}$  incidence. The results (tabulated in Table 3) were treated as before, except that corrections for wavemaking resistance were applied to three columns instead of two. The drag is plotted against the velocity in figure 6, showing good agreement with  $C_{\rm d} = 1.49$ , close to the corresponding result for zero degrees of incidence. For reasons discussed next, it seems likely that this represents an over-estimate of the true drag coefficient.

### 3.4 Blockage effects

Very little is known about blockage effects on the drag of a surface-piercing bluff body. In the present experimental arrangements the frontal area of the model represented 5.1% of the water cross section, and at similar 'total blockage ratios' in a closed wind tunnel Farell et al. [8] measured increases of about 30% in the base suction coefficient on cooling towers (Fig. 10 in ref. [8]), but increases in sectional drag coefficients of less than 4% (Fig.12 in ref. [8]). In measurements of base suction coefficients in open-jet tunnels (in which, rather more like

the present case, the flow can expand around the body and its wake) there was almost no change in the pressure distribution at total blockage ratios of up to 10% (Fig.10 in ref. [8]). It seemed unlikely therefore that blockage effects in the present case would generate an increase of more than 4% in the drag coefficient, but to investigate the question further some additional measurements were carried out in the first series of tests with false side walls mounted on the carriage to reduce the effective width of the flume from 1.71m to 1.31m. Under these conditions the model's drag coefficient was found to increase by 4.4% from 1.47 to 1.53, adding support to the conclusion that the blockage effect at a width of 1.71m was not more than 4%.

## 4. CLOSING REMARKS

The measurements of the drag force on the model TLP presented in this note are intended to aid in quantifying the uncertainty in the results obtained by using computational fluid dynamics to assess the hydrodynamic loading full-scale offshore structures. The geometry of the model TLP is well defined (Fig. 1 and Table 1) and construction of a computational mesh to resolve the flow around it should pose no difficulty to any of the grid-generation tools available to the offshore engineering community. Upstream of the TLP, where inlet conditions will need to be specified in the computations, the flow conditions are also well defined, consisting of uniform mean-flow velocity along the flume's length with no appreciable secondary flow in the perpendicular plane. The turbulence intensity is low. The model TLP was located at distance of five column heights from the flume bed and hence a slip boundary condition can be applied thereby obviating the need to resolve the near-wall region. Similarly, wavemaking resistance was accounted for in the reported results and hence the rigid-lid approximation can be applied to specify the free stream boundary conditions. The principal results from CFD simulations at both 0° and 45° incidence should yield values of the drag coefficient that are in the range 1.20 - 1.25 with the 4% spread being due to the inevitable blockage effects in the experiments.

#### REFERENCES

1. Wu, G., Jang, H., Kim, J. W., Ma, W., Wu, M-C, and O'Sullivan, J. (2014) Benchmark of CFD modelling of TLP free motion in extreme wave event. *Proc. ASME 33<sup>rd</sup> Int. Conf. on* 

- Ocean, Offshore and Arctic Engineering, June 8-13 2014, San Francisco, Paper number OMAE2014-24658
- 2. Tan, J. H. C., Magee, A., Kim, J. W., Teng, Y. J., Zakni, N. A. (2013) CFD simulation for vortex induced motions of a multi-column floating platform. *Proc. ASME 32<sup>nd</sup> Int. Conf. on Ocean, Offshore and Arctic Engineering*, June 9-14 2013, Nantes, Paper number OMAE2013-11117
- 3. Younis, B. A., and Przulj, V. P. (2006) Prediction of hydrodynamic loading on a mini TLP with free surface effects. *Ocean Engineering*, 33 (2), 181-204.
- 4. Younis, B. A. & Abrishamchi, A. (2014). Three-dimensional turbulent vortex shedding from a surface-mounted square cylinder: predictions with Large-Eddy Simulations and URANS. *Trans. ASME J. Fluids Engineering*, 136 (6), Article number: 060907.
- 5. Teigen, P., Przulj, V. P. and Younis, B. A. (1999) A CFD investigation into the effects of current incidence on the hydrodynamic loading on a deepwater TLP. *J. Offshore Mechanics and Arctic Engineering*, 121 (2), 109-115.
- 6. Qui, W., Junior, J. S., Lee, D., Lie, H., Magarovskii, V., Mikami, T., Rousset, J-M, Sphaier, S., Tao, L., Wang, X. (2014). *Ocean Engineering*, 86, 58-67.
- 7. Chaplin J R and Teigen P (2003). Steady flow past a vertical surface-piercing circular cylinder. *J. Fluids and Structures*, 18 (3), 271-285.
- 8. Farell, C., Carrasquel, S., Guven, O. and Patel, V.C. (1977). Effect of wind-tunnel walls in the flow past circular cylinder and cooling tower models. *Trans. ASME J. Fluids Engineering*, 99 (3), 470–479.

	Full-scale TLP	Towing-tank model
Column height H (m)	22.25	0.32
Column diameter D (m)	8.75	0.125
Columns separation (m)	28.50	0.407
Pontoon height B (m)	6.25	0.089
Draught (H+B) (m)	28.50	0.407

Table 1: Dimensions of full-scale TLP and towing-tank model.

Re	$C_d$
16947	1.5720
24704	1.3560
28237	1.2560
33442	1.2130
36220	1.1930
37747	1.2100
43586	1.2010
48864	1.3960
55829	1.2010
60573	1.1960
63939	1.2110
65315	1.2160
71223	1.2090
76410	1.2390
81574	1.2670
84466	1.2890
90909	1.3210
94461	1.3360

Table 2: Drag coefficients for 0° incidence.

Re	$C_d$
Re	Cd
40453	1.490
47298	1.605
48245	1.574
51337	1.474
54193	1.491
54543	1.490
62763	1.406
66765	1.435
70818	1.443
75259	1.453
79538	1.471
83335	1.471
87689	1.478
91847	1.490
97955	1.470

Table 3: Drag coefficients for 45° incidence.

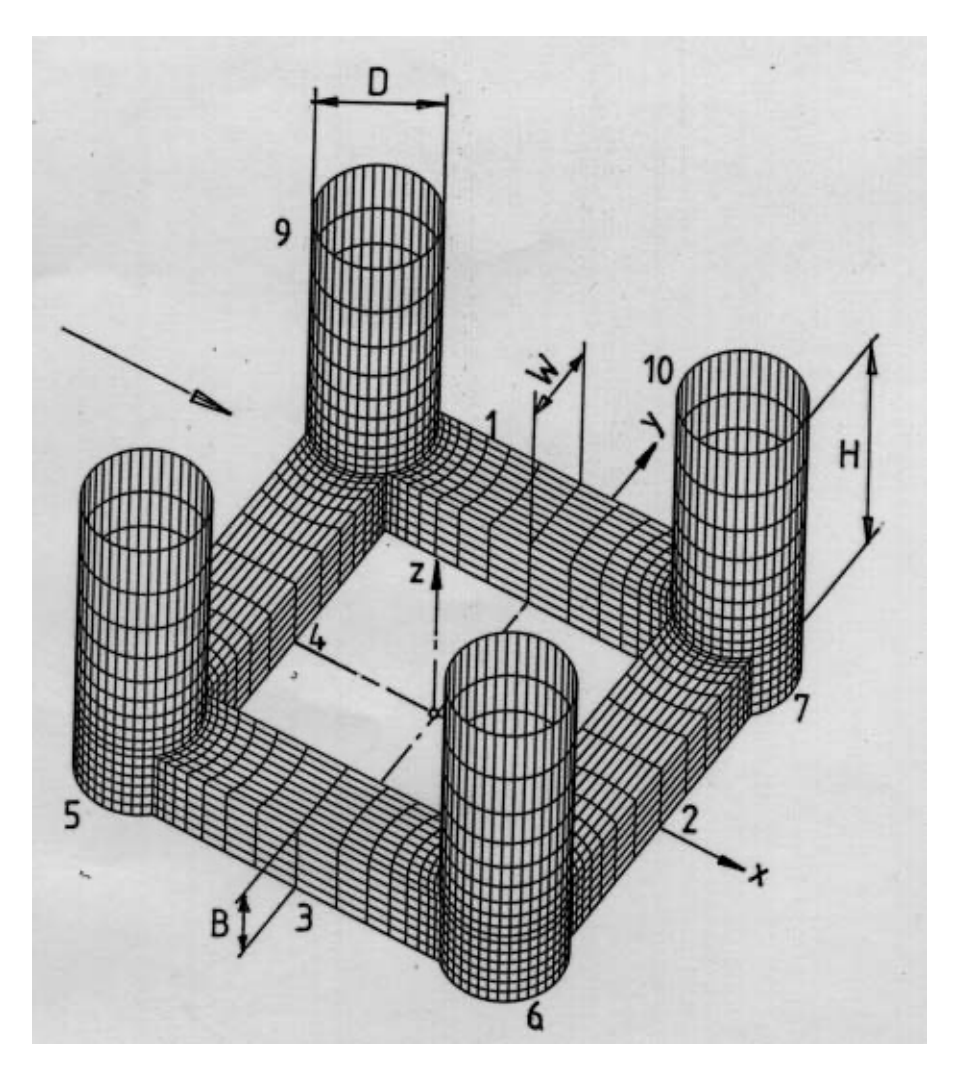
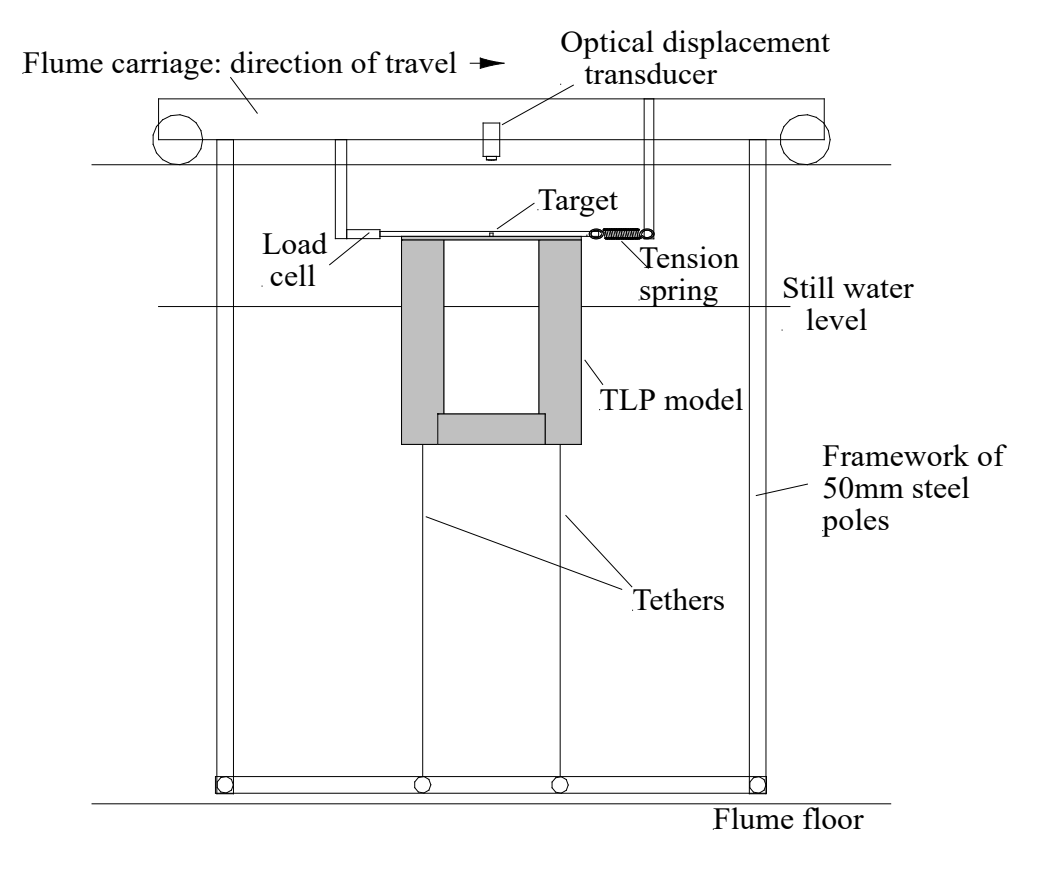


Figure 1. Schematic of model TLP



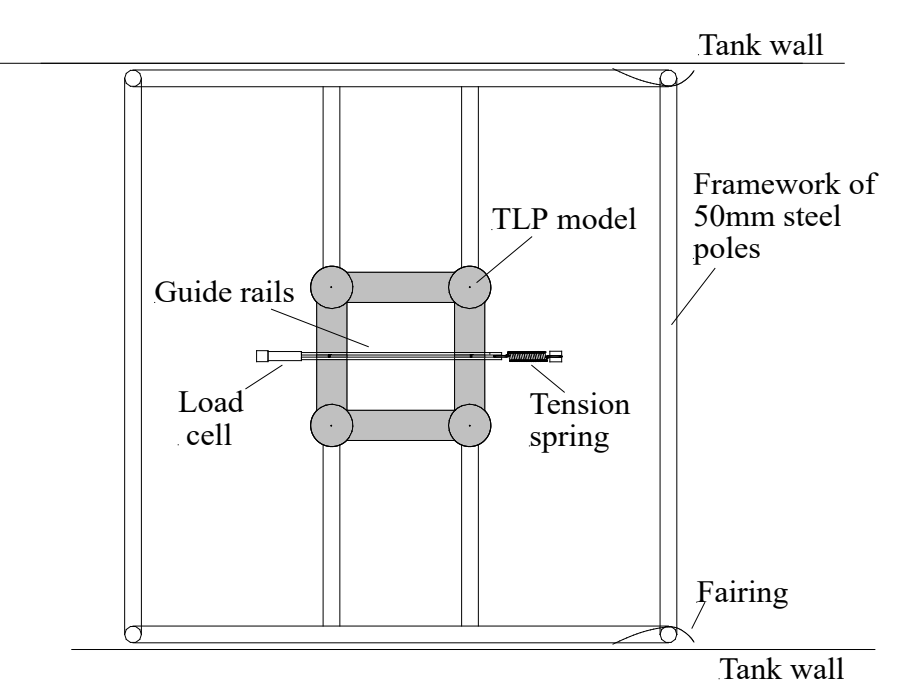


Figure 2. Elevation (above) and plan (below) views of the model TLP mounted in the towing flume. The first series of tests made use of the optical displacement transducer to measure the model's displacement against the tension spring. In the second series, the drag was measured directly with the load cell.

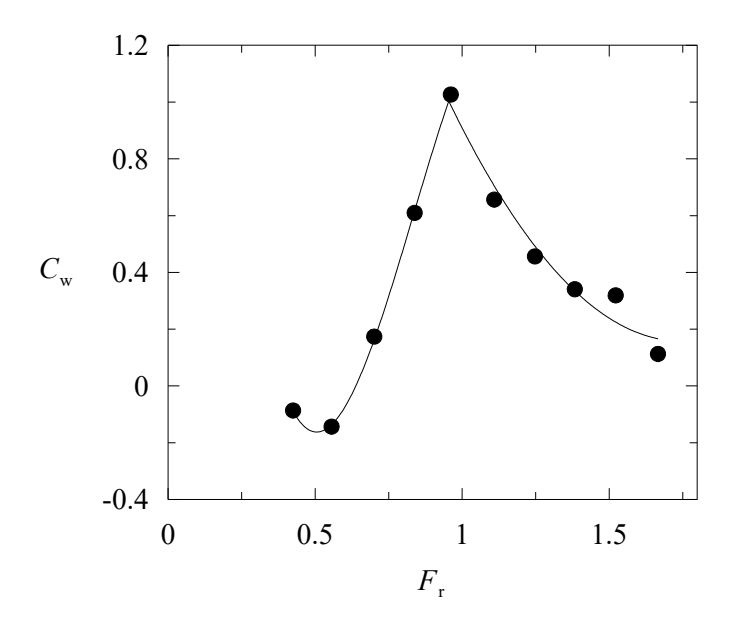


Figure 3. Wavemaking resistance coefficient for a vertical surface-piercing cylinder at constant speed (Chaplin & Teigen, 2000). Lines represent separate polynomial fits for  $F_r < 1$  and  $F_r > 1$ .

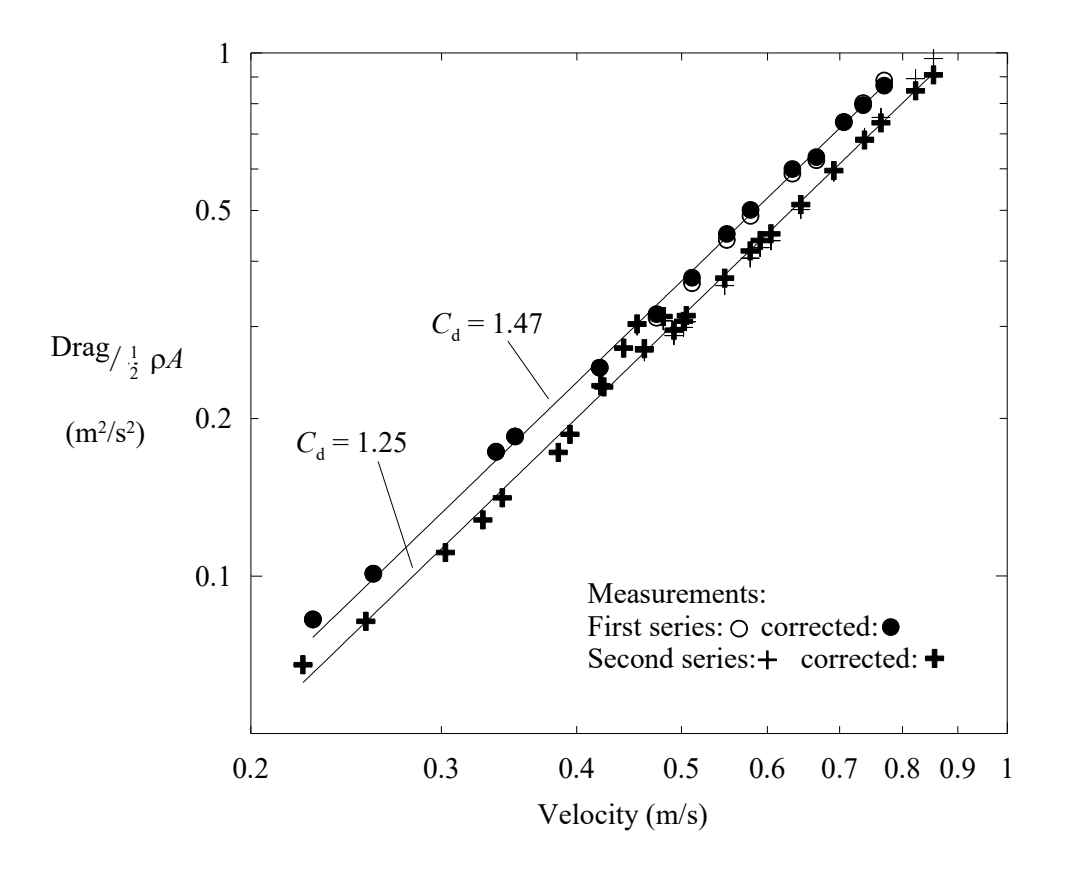


Figure 4. Drag plotted against velocity for zero incidence. The data are shown with and without corrections for wavemaking resistance.

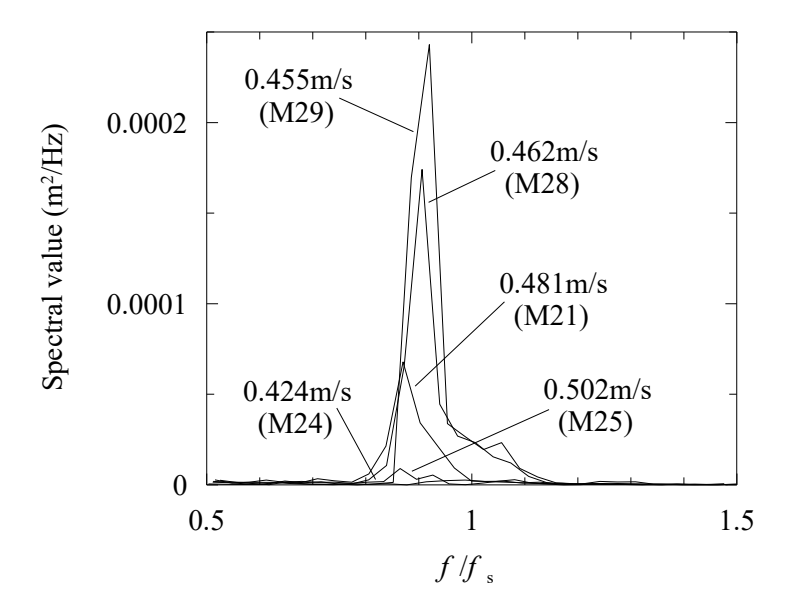


Figure 5. Spectra of water surface elevation records measured in the wake of the model at various speeds.

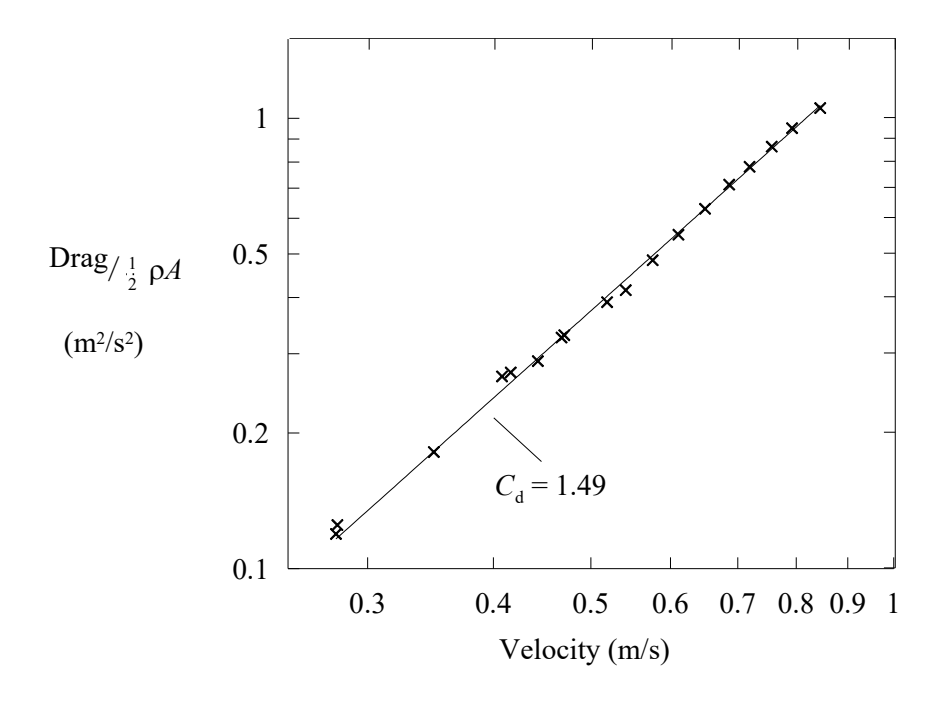


Figure 6. Drag at 45° incidence.